University of Udine

Department of Mathematics and Computer Science

PREPRINT

The environment and distribution of emitting electrons as a function of source activity in Markarian 421

Mankuzhiyil N., Ansoldi S., Persic M., Tavecchio F.

THE ENVIRONMENT AND DISTRIBUTION
OF EMITTING ELECTRONS
AS A FUNCTION OF SOURCE ACTIVITY
IN MARKARIAN 421

Nijil Mankuzhiyil[1]

Dipartimento di Fisica, Università di Udine, via delle Scienze 208, I-33100 Udine (UD), ITALY

Stefano Ansoldi[1,2]

International Center for Relativistic Astrophysics (ICRA)

Massimo Persic[1]

INAF-Trieste, via G. B. Tiepolo 11, I-34143 Trieste (TS), ITALY

Fabrizio Tavecchio

INAF-Brera, via E. Bianchi 46, I-23807 Merate (LC), ITALY

---

[1]and INFN Sezione di Trieste

[2]and Dipartimento di Matematica e Informatica, Università di Udine, via delle Scienze 206, I-33100 Udine (UD), ITALY

ABSTRACT

For the high-frequency peaked BL Lac object Mrk 421 we study the variation of the spectral energy distribution (SED) as a function of source activity, from quiescent to active. We use a fully automatized χ^2-minimization procedure, instead of the "eyeball" procedure more commonly used in the literature, to model nine SED datasets with a one-zone Synchrotron-Self-Compton (SSC) model and examine how the model parameters vary with source activity. The latter issue can finally be addressed now, because simultaneous broad-band SEDs (spanning from optical to VHE photon energies) have finally become available. Our results suggest that in Mrk 421 the magnetic field (B) decreases with source activity, whereas the electron spectrum's break energy (γ_{br}) and the Doppler factor (δ) increase – the other SSC parameters turn out to be uncorrelated with source activity. In the SSC framework these results are interpreted in a picture where the synchrotron power and peak frequency remain constant with varying source activity, through a combination of decreasing magnetic field and increasing number density of $\gamma \leq \gamma_{\mathrm{br}}$ electrons: since this leads to an increased electron-photon scattering efficiency, the resulting Compton power increases, and so does the total (= synchrotron plus Compton) emission.

Subject headings: BL Lacertae objects: general – BL Lacertae objects: individual (Mrk 421) – diffuse radiation – gamma rays: galaxies – infrared: diffuse background

1. Introduction

It's commonly thought that the fueling of supermassive black holes, hosted in the cores of most galaxies, by surrounding matter produces the spectacular activity observed in AGNs. In some cases ($\lesssim 10\%$) powerful collimated jets shoot out in opposite directions at relativistic speeds. The origin of such jets is one of the fundamental open problems in astrophysics.

If a relativistic jet is viewed at small angle to its axis, the observed emission is amplified by relativistic beaming (Doppler boosting and aberration) allowing deep insight into the physical conditions and emission processes of relativistic jets. Sources whose boosted jet emission dominates the observed emission (blazars[1]) represent a minority among AGN, but are the dominant extragalactic source class in γ-rays. Since the jet emission overwhelms all other emission from the source, blazars are key sources for studying the physics of relativistic extragalactic jets.

The jets' origin and nature are still unclear. However, it is widely believed that jets are low-entropy (kinetic/electromagnetic) flows that dissipate some of their energy in (moving) regions associated with internal or external shocks. This highly complex physics is approximated, for the purpose of modelling the observed emission, with one or more relativistically moving homogeneous plasma regions (blobs), where radiation is emitted by a non-thermal population of particles (e.g. Maraschi et al. 1992). The high energy emission, with its extremely fast and correlated multifrequency variability, indicates that often one single region dominates the emission.

The jet's broad-band (from radio to γ-ray frequencies) spectral energy distribution (SED) is a non thermal continuum featuring two broad humps that peak at IR/X-ray and GeV/TeV

---

[1]Within the blazar class, extreme objects, lacking even signatures of thermal processes usually associated with emission lines, are defined as BL Lac objects.

frequencies and show correlated luminosity and spectral changes. This emission is commonly interpreted within a Synchrotron-Self-Compton (SSC) model where the synchrotron and Compton peaks are produced by one same time-varying population of particles moving in a magnetic field (e.g., Tavecchio et al. 1998, hencefort T98). The SSC model is perfectly adequate to explain the SEDs of BL Lac sources (e.g., Tavecchio et al. 2010).

One important issue that should be addressed, but has not yet been so far because of the lack of simultaneous broad-band SEDs, is how the emission changes as a function of the source's global level of activity. In particular, given an emission model that fits the data, it is should be examined what model parameters are correlated with source activity. In order to investigate SEDs at different levels of activity we choose a high-frequency-peaked BL Lac (HBL) object, i.e. a blazar (i) whose relativistic jet points directly toward the observer, so owing to relativistic boosting its SSC emission dominates the source; (ii) whose Compton peak ($\gtrsim 100\,\mathrm{GeV}$) can be detected by Cherenkov telescopes; and (iii) whose GeV spectrum can be described as a simple power law (unlikely other types of BL Lacs, see Abdo et al. 2009). In addition, such HBL source must have several simultaneous SED datasets available. Mrk 421 meets these requirements. In this paper we study the variation of its SED with source activity, from quiescent to active.

Another requirement for this kind of study concerns the modeling procedure. We use a full-fledged χ^2-minimization procedure instead of the "eyeball" fits more commonly used in the literature. While the latter at most prove the existence of a *good* solution, by finely exploring the parameter space our procedure finds the *best* solution and also proves such solution to be *unique*.

In this paper we investigate the SED of Mrk 421 in nine different source states. To this aim we fit a one-zone SSC emission model (described in Sect.3) to the data using a fully automatized χ^2-minimization procedure (Sect.3). The results are presented and discussed in Sect.4.

2. BL Lac SSC emission

To describe the HBL broad-band emission, we use the one-zone SSC model of T98. This has been shown to adequately describe broad-band SEDs of most high-frequency-peaked BL Lac objects (e.g., Tavecchio et al. 2010) and, for a given source, both its ground and excited states (Tavecchio et al. 2001; Tagliaferri et al. 2008). The main support for the one-zone model is that in most such sources the temporal variability is clearly dominated by one characteristic timescale, which implies one dominant characteristic size of the emitting region (e.g., Anderhub et al. 2009). Moreover, one of the most convincing evidence favoring the SSC model is the strict correlation that usually holds between the X-ray and VHE γ-ray variability (e.g., Fossati et al. 2008): since in the SSC model the emission in the two bands is produced by the same electrons (via synchrotron and SSC mechanism, respectively), a strict correlation is expected[2].

In our work, for simplicity we used a one-zone SSC model, assuming that the entire SED is produced within a single homogeneous region of the jet. As already noted, this class of models is generally adequate to reproduce HBL SEDs. However, one-zone models also face some problems in explaining some specific features of TeV blazar emission. In particular, while very large Doppler factors are often required in one-zone model, radio VLBI observations hardly detect superluminal motion at parsec scale (e.g., (Piner et al. 2010; Giroletti et al. 2006)). This led (Georganopoulos & Kazanas 2003; Ghisellini et al. 2005) to propose the existence of a structured, inhomogeneous and decelerating emitting jet. Inhomogeneous (two-zone) models (e.g., (Ghisellini & Tavecchio 2008)) have been also invoked to explain the ultra-rapid variability occasionally observed in TeV blazars (e.g., (Aharonian et al. 2007; Albert et al. 2007).

The emission zone is supposed to be spherical with radius R, in relativistic motion

[2]The rarely occurring "orphan" TeV flares, that are not accompanied by variations in the X-ray band, may arise from small, low-B, high-density plasma blobs (Krawczynski et al. 2004).

with bulk Lorentz factor Γ at an angle θ with respect to the line of sight to the observer, so that special relativistic effects are cumulatively described by the relativistic Doppler factor, $\delta = [\Gamma(1 - \beta\cos\theta)]^{-1}$. Relativistic electrons with density n_e and a tangled magnetic field with intensity B homogeneously fill the region.

The relativistic electrons' spectrum is described by a smoothed broken power-law function of the electron Lorentz factor γ, with limits γ_1 and γ_2, break at γ_{br} and low- and high-energy slopes n_1 and n_2. This purely phenomenological choice is motivated by the observed shape of the humps in the SEDs, well represented by two smoothly joined power laws for the electron distribution. Two ingredients are important in shaping the VHE γ-ray part of the spectrum: (i) using the Thomson and Klein-Nishina cross sections when, respectively, $\gamma h\nu \leq m_e c^2$ and $\gamma h\nu > m_e c^2$ (with ν the frequency of the 'seed' photon), in building the model (T98); and (ii) the correction of $\gtrsim 50\,\text{GeV}$ data for absorption by the Extragalactic Background Light (EBL), as a function of photon energy and source distance (e.g., Mankuzhiyil et al. 2010, and references therein): for this purpose we use the popular Franceschini et al. (2008) EBL model.

The one-zone SSC model can be fully constrained by using simultaneous multifrequency observations (e.g., T98). Of the nine free parameters of the model, six specify the electron energy distribution (n_e, γ_1, γ_{br}, γ_2, n_1, n_2), and 3 describe the global properties of the emitting region (B, R, δ). Ideally, from observations one can derive six observational quantities that are uniquely linked to model parameters: the slopes, $\alpha_{1,2}$, of the synchrotron bump at photon energies below and above the UV/X-ray peak are uniquely connected to $n_{1,2}$; the synchrotron and SSC peak frequencies, $\nu_{s,C}$, and luminosities, $L_{s,C}$, are linked with B, n_e, δ, γ_{br}; finally, the minimum variability timescale t_{var} provides an estimate of the source size through $R \lesssim c\,t_{var}\delta/(1+z)$.

To illustrate how important it is to sample the SED around *both* peaks, let us consider a standard situation before Cherenkov telescopes came online, when we would have had only knowledge of the UV/X-ray (synchrotron) peak. Clearly this would have given us information on

the shape of the electron distribution but would have left all other parameters unconstrained: in particular the degeneracy between B and n_{e} – inherent in the synchrotron emissivity – could not be lifted without the additional knowledge of the HE/VHE γ-ray (Compton) peak.

Therefore, only knowledge of observational quantities related to both SED humps enables determination of all SSC model parameters.

3. χ^2 minimization

In this section we discuss the code that we have used to obtain an estimation of the characteristic parameters of the SSC model. As we recalled in the previous section the SSC model that we are assuming is characterized by nine free parameters, n_{e}, γ_1, γ_{br}, γ_2, n_1, n_2, B, R, δ. However, in this study we set $\gamma_1 = 1$, which is a widespread assumption in the literature, so reducing the number of free parameters to eight.

The determination of the eight free parameters has been performed by finding their best values and uncertainties from a χ^2 minimization in which multi-frequency experimental points have been fitted to the SSC model described in T98. Minimization has been performed using the Levenberg–Marquardt method (see Press et al. 1994), which is an efficient standard for non-linear least-squares minimization that smoothly interpolates between two different minimization approaches, namely the inverse Hessian method and the steepest descent method.

The algorithm starts by making an educated guess for a starting point P_0 in parameter space with which the minimization loop is entered; at the same time a (small) constant is defined, $\Delta\chi^2_{\mathrm{NI}}$ (where NI stands for Negligible Improvement), which represents an increment in χ^2 small enough that the minimization step can be considered to have achieved no significative improvement in moving toward the minimum χ^2: this will be used as a first criterion for the exit condition from the minimization loop. Indeed, to be more confident that the minimization loop has reached a χ^2

value close enough to the absolute minimum, the above condition has to be satisfied four times in a row: the number of consecutive times the condition has been satisfied is conveniently stored into the integer variable c_{NI} – which is, thus, set to zero at startup. From the chosen value of P_0 we can compute the associated $\chi_0^2 = \chi^2(P_0)$ and enter the minimization loop. The Levenberg-Marquardt method will determine the next point in parameter space, P, where χ^2 will be evaluated. If $\chi^2(P) > \chi_0^2$ the weight of the steepest-descent method in the minimization procedure is increased, the variable c_{NI} is set to zero, and we can proceed to the next minimization step. If, instead, $\chi^2 \leq \chi_0^2$ we further check if the decrease in χ^2 is smaller than or equal to $\Delta\chi_{\mathrm{NI}}^2$. If this is the case, the negligible-improvement counter c_{NI} is increased by one: if the resulting value is $c_{\mathrm{NI}} \geq 4$, we think we have a good enough approximation of the absolute minimum – and the algorithm ends. If, instead, in the latter test $c_{\mathrm{NI}} < 4$, or if in the preceding test $\Delta\chi^2 > \Delta\chi_{\mathrm{NI}}^2$, then we increase the weight of the inverse Hessian method in the minimization procedure, we set χ_0^2 equal to the lower value we have just found, and we continue the minimization loop. For completeness and illustration , we briefly present the flow-chart of the algorithm in Fig. 1.

A crucial point in our implementation is that from T98 we can only obtain a numerical approximation to the SSC spectrum, in the form of a sampled SED. On the other hand, at each step of the loop (see Fig. 1) the calculation of χ^2 requires the evaluation of the SED for all the observed frequencies. Usually the model function is known analytically, so these evaluations are a straightforward algebraic process. In our case, instead, we know the model function only through a numerical sample and it is unlikely that an observed point will be one of the sampled points coming from the implementation of the T98 model. Nevertheless it will in general fall between two sampled points, which allows us to use interpolation[3] to approximate the value of the SED.

At the same time, the Levenberg–Marquardt method requires the calculation of the partial

---

[3]The sampling of the SED function derived from T98 is dense enough, so that, with respect to other uncertainties, the one coming from this interpolation is negligible.

derivatives of χ^2 with respect to the eight fitted SSC parameters. Contrary to the usual case, in which from the knowledge of the model function all derivatives can be obtained analytically, in our case they have also been obtained numerically by evaluating the incremental ratio of the χ^2 with respect to a sufficiently small, dynamically adjusted increment of each parameter. This method could have introduced a potential inefficiency in the computation, due to the recurrent need to evaluate the SED at many, slightly different points in parameter space, this being the most demanding operation in terms of CPU time. For this reason we set up an algorithm to minimize the number of calls to T98 across different iterations.

4. Datasets

From the literature we then select nine SED datasets corresponding to different emission states (low to high) of the HBL source Mrk 421.

State 1 and state 2 (Acciari et al. 2009) multi-wavelength campaigns were triggered by a major outburst in April 2006 that was detected by the *Whipple* 10 m telescope. A prompt campaign was not possible because of visibility constraints on XMM-*Newton*. So simultaneous multi-wavelength observations took place during the decaying phase of the burst. The optical/UV and X-ray observations were carried out using XMM-*Newton*'s optical monitor (OM) and EPIC-pn detector, respectively. The MAGIC and *Whipple* telescopes were used for the VHE γ-ray observations. State 1 strictly simultaneous observations lasted $\sim$4 hrs for state 1, and more than 3 hrs for state 2.

State 3 (Rebillot et al. 2006) reports the multi-wavelength observations during December 2002 and January 2003. The campaign was initiated by X-tay and VHE flares detected by the All Sky Monitor (ASM) of the *Rossi* X-ray Timing Explorer (*R*XTE) and the 10 m *Whipple* telescope. *Whipple* and HEGRA-CT1 were used for the VHE observations during the campaign.

Even though *Whipple* observed the source from Dec.4, 2002 to Jan.15, 2003, and HEGRA-CT1 on Nov.3–Dec.12, 2002, only the data taken during nights with simultaneous X-ray observations are used in this paper to construct the SED. Optical flux is the average flux of the data obtained from Boltwood observatory optical telescope, KVA telescope, and WIYN telescope during the campaign period.

State 4 and state 9 (Blazejowski et al. 2005) observations were taken from a comparatively longer time campaign in 2003 and 2004. The X-ray flux obtained from *R*XTE were grouped into low-, medium- and high-flux groups. For each X-ray observation in a given group, *Whipple* VHE γ-ray data that had been observed within an hour of the X-ray data was selected. State 4 (i.e., medium-flux) was observed between March 8 and May 3, 2003; whereas state 9 (i.e., high-flux) was observed on April 16-20, 2004. Optical datasets obtained with *Whipple* Observatory's 1.2 m telescope and Boltwood Observatory's 0.4 m telescope were also selected based on the same grouping method. The optical data measured during the whole campaign were not simultaneous with the other multi-wavelength data: however, the optical flux was not found to vary significantly during the campaign, so its highest and lowest values are taken to be reliable proxies of the actual values.

State 5 and state 7 (Fossati et al. 2008) data were taken on March 18-25, 2001 during a multi-wavelength campaign. State 7 denotes the peak of the March 19 flare, whereas state 5 denotes a post-flare state on March 22 and 23. In both cases the X-ray and VHE γ-ray data were obtained with, respectively, *R*XTE and the *Whipple* telescope. The lowest and highest optical fluxes obtained during the whole campaign with the 1.2 m Harvard-Smithsonian telescope on Mt. Hopkins were used in the SEDs for states 5 and 7, respectively.

State 6 (Acciari et al. 2009) observations were taken, using the same optical and X-ray instruments as states 1 and 2, during a decaying phase of an outburst in May 2008. The VHE γ-ray data were taken with VERITAS. There are $\sim$2.5 hours of strictly simultaneous data.

State 8 (Donnarumma et al. 2009) data were taken during a multi-wavelength campaign on June 6, 2008: VERITAS, *R*XTE and Swift/BAT, and WEBT provided the VHE γ-ray, X-ray, and optical data, respectively.

5. Results and discussion

To each of the datasets we apply our χ^2-minimization procedure (see Fig. 1). The best-fit SSC models are plotted alongside the SED data in Fig. 2.

Obtaining truly best-fit SSC models of simultaneous blazar SEDs is crucial to measure the SSC parameters describing the emitting region. The obtained optimal model is proven to be unique because the SSC manifold is thoroughly searched for the absolute χ^2 minimum. Furthermore, the very nature of our procedure ensures that there is no obvious bias affecting the resulting best-fit SSC parameters.

Nevertheless, as it has also been discussed (Andrae et al. 2010), there may be caveats related with the χ^2_ν fitting, especially when applied to non-linear models such as the present one. For this reason, it is important to try to understand the goodness of the fit with methods other than the value of χ^2_ν (reported in table 1). Following (Andrae et al. 2010), we have applied the Kolmogorov-Smirnov (KS) test for normality of the residuals of all our SED fits. A standard application of the test shows that in all cases the residuals are *not* normally distributed: the KS test thus fails at the 5% significance level. It is, of course, crucial to understand the reason for this behavior of our SSC fits with respect to the KS test. Let us start with some general remarks about the modelling of blazar emission and their observations. First, the one zone SSC model contains two distinct physical processes in one same region, i.e. synchrotron emission and its Compton up-scattered counterpart, that manifest themselves as essentially separate components at very different energies; on the other hand, additional subtle effects may enter the modelling of

blazar emission, so that the SSC model may only be an approximation to the real thing. (A more refined KS analysis suggests exactly this, see below). Second, our blazar datasets do cover the (far apart) energy ranges spanned by, respectively, the synchrotron and Compton emission: but they markedly differ in these two spectral regions, in that the uncertainties associated with VHE data are much larger than those associated with the optical and X-ray data.

Both these observations suggest us and give us the possibility of a slightly different approach to the problem of the statistical significance of the fits, which will turn out to be quite enlightening. We will refer to this other approach as the *piecewise KS test*: it consists in applying the KS test, separately to low energy and high energy data (see Appendix). The main motivation behind this idea is, as discussed above, the marked difference, from both the physical and the data-quality point of view, of the lower and higher energy ranges. Surprisingly, if for each SED we separately check the low- and high-energy residuals for normality, the KS test always confirms their (separate) normality at the 5% confidence level. On the technical side we took all the necessary precautions to improve reliability: the null hypothesis statistics have been obtained from a Montecarlo simulation of 100,000 datasets having the same dimension as the residuals datasets. Critical values to test normality of the residuals have been obtained from these numerically determined statistics and, normality holds in all that cases we have considered. Hence, it is unlikely to be a coincidence, and this calls for an explanation. Clearly, the fact that the piecewise KS test is not able to reject the normality of the low-/high-energy residuals separately, means that the fitted SEDs can be considered as a reasonable models separately at low and high energies. Of course, because of the quality of especially high energy data, the uncertainties on the parameters of the fit are sometimes quite large, a fact that unfortunately can not be avoided, despite the fact that the quality of the datasets that we are using is certainly above average among those that are available. At the same time, the failure for normality of the residuals on the standard KS test, in which low- and high-energy residuals are considered simultaneously, suggests that existing data may require the SSC model to be improved – perhaps by taking into account higher-order effects

(e.g., two- or multiple-zone emission, additional soft photons other than the synchrotron ones, and/or hadronic effects). So, and with more and better VHE data available, it could be possible to reduce the uncertainties in the parameters and to obtain a higher overall significance in the fit.

Given the above, the results found with our fits are the best possible in the framework of existing datasets and models of blazar emission: at least, they have a quantitative and clear statistical meaning. Therefore, we think it is useful to examine some possible consequences of the results derived from the above fits – we'll do so in what follows.

In Tables 1, 2 we report the best-fit SSC parameters. Source activity (measured as the total luminosity of the best-fit SSC model) appears to be correlated with B, γ_{br}, and δ (see Fig. 3-*top*) – and to be uncorrelated with the remaining SSC parameters. The bolometric luminosity used in these plots has been obtained directly from the fitted SED. In more detail, after determining the numerical approximation to the SED $\log[\nu F(\nu)]$, the parameters being fixed at their best values obtained with the previously described minimization procedure, we have performed $L = \int_{\nu_{\min}}^{\nu_{\max}} \nu F(\nu) d\nu$, with $\nu_{\min}$, $\nu_{\max}$ set at 2.5 decades, respectively, below the synchrotron peak and above the Compton peak. In this way we make sure to perform the integral over all the relevant frequencies in a way that is independent from any in location of these peaks.

Coherently with our approach in the former part of this paper, we searched the data plotted in the top row of Fig. 2 for possible correlations. The linear-correlation coefficients turn out to be 0.67, 0.64 and 0.54, which confirm linear correlations with confidence levels of 4.8%, $6, 3\%$ and $13, 3\%$, respectively. As an additional test (given the relatively low statistics of our datasets), we checked that the KS test confirms normality of the fit residuals[4].

All the parameters derived through our automatic fitting procedure are within the range of

---

[4]The same approach involving a Montecarlo generated empirical distribution for the null-hypothesis described just above has been used also in all these cases.

SSC parameters found in the literature for HBLs in general (e.g. (Tavecchio et al. 2001, 2010; Tagliaferri et al. 2008; Celotti & Ghisellini 2008)) and for Mrk 421 in particular (e.g., (Bednarek & Protheroe 1997; Tavecchio et al. 1998; Maraschi et al. 1999; Ghisellini et al. 2002; Konopelko et al. 2003; Fossati et al. 2008)). In particular, large Doppler factors such as those derived in our extreme cases, $\delta > 50$, have been occasionally derived (e.g., (Konopelko et al. 2003; Fossati et al. 2008); see also the discussion in (Ghisellini et al. 2005)).

As is seen from Fig. 3-*top*, $\gamma_{\rm br}$ and B are correlated, respectively, directly (*left*) and inversely (*right*) with L. This may be explained as follows. An increase of $\gamma_{\rm br}$ implies an effective increase of the energy of most electrons (or, equivalently, of the density of $\gamma < \gamma_{\rm br}$ electrons). To keep the synchrotron power and peak roughly constant (within a factor of 3; see Fig. 2), B must decrease. This improves the photon-electron scattering efficiency, and the Compton power increases. The total (i.e., synchrotron plus Compton) luminosity will be higher. So a higher $\gamma_{\rm br}$ implies a lower B and a higher emission state. The δ–L correlation (Fig. 3–*top-middle*) results from combining the B–δ inverse correlation (Fig. 3–*bottom-right*; see below) and the B–L anticorrelation.

A deeper insight on emission physics can be reached plotting the three L-dependent parameters one versus the other (Fig. 3-*bottom*). The B–$\gamma_{\rm br}$ anticorrelation, with $\Delta \log {\rm B} \simeq -2 \, \Delta \log \gamma_{\rm br}$ (Fig. 3–*bottom-left*), derives from the synchrotron peak, $\nu_{\rm s} \propto B\gamma^2$, staying roughly constant (see Fig. 2). For fixed synchrotron and Compton peak frequencies in a relativistically beamed emission, the B–δ relation is predicted to be inverse in the Thompson limit and direct in the Klein-Nishina limit (e.g., Tavecchio et al. 1998): because $\nu_{\rm s}$, $\nu_{\rm c}$ do not greatly vary from state to state in our data (see Fig. 2), the correlation in Fig. 3–*bottom-right* suggests that the Compton emission of Mrk 421 is always in the Thompson limit. The δ–$\gamma_{\rm br}$ correlation (Fig. 3–*bottom-middle*) results as a corollary of the condition of constant $\nu_{\rm s}$, $\nu_{\rm c}$ emitted by a plasma in bulk relativistic motion toward the observer.

Our fits show clear trends among some of the basic physical quantities of the emitting region,

the magnetic field, the electron Lorentz factor at the spectral break, and the Doppler factor (see Fig. 3). In particular, B and γ_{break} follow a relation $B \propto \gamma_{\mathrm{break}}^{-2}$, while B and δ are approximately related by $B \propto \delta^{-2}$.

Rather interestingly, the relation connecting B and γ is naturally expected within the context of the simplest electron acceleration scenarios (e.g., (Henri et al. 1999)). In this framework, the typical acceleration timescale, t_{acc}, is proportional to the gyroradius: $t_{\mathrm{acc}}(\gamma) \propto r_{\mathrm{L}}/c$, where $r_{\mathrm{L}} = \gamma m_e c/(eB)$ is the Larmor radius. On the other hand, acceleration competes with radiative (synchrotron and IC) cooling. In Mrk 421, characterized by comparable power in the synchrotron and IC components, we can assume that $t_{\mathrm{cool}}(\gamma) \approx t\mathrm{syn} \propto 1/\gamma B$. The maximum energy reached by the electrons is determined by setting these two timescales equal, i.e.

$$t_{\mathrm{acc}}(\gamma_{\mathrm{max}}) = t_{\mathrm{cool}}(\gamma_{\mathrm{max}}) \;\rightarrow\; \gamma_{\mathrm{max}} \propto B^{-1/2}\,, \tag{1}$$

in agreement with the relation derived by our fit. It is therefore tempting to associate γ_{break} to γ_{max} and explain the $B \propto \gamma_{\mathrm{break}}^{-2}$ relation as resulting from the acceleration/cooling competition.

If the above inference is correct, one can explain the variations of γ_{break} as simply reflecting the variations of B in the acceleration region. In turn, the variations of B could be associated either to changes in the global quantities related to the jet flow or to some local process in the jet (i.e. dissipation of magnetic energy through reconnection). The second relation mentioned above, i.e. δ vs. B, seems to point to the former possibility. First of all let us assume $\delta \sim \Gamma$ (since we are probably observing the Mrk 421 jet at a small angle w.r.t. the line of sight). A general result of jet acceleration models is that, during the acceleration phase, the jet has a parabolic shape, $R \propto d^{1/2}$ (with d the distance from the central black hole), and the bulk Lorentz factor Γ increases with d as $\Gamma \propto d^{1/2}$ (e.g., (Vlahakis & Königl 2004; Komissarov et al. 2007)). On the other hand, if the magnetic flux is conserved, $B \propto R^{-2} \propto d^{-1}$ and thus we found $B \propto \Gamma^{-2}$. Albeit somewhat speculative, these arguments suggest that the trends displayed in Fig. 3 are naturally expected in the general framework of jet acceleration.

The correlations in Fig. 3-*bottom* seem to be tighter than those in Fig. 3-*top*. The larger scatter affecting the latter owes to the fact that the electron density, n_e, that also enters the definition of SSC luminosity, shows no correlation with B, $\gamma_{\rm br}$, and δ – hence it slightly blurs the latter's plots with luminosity.

One further note concerns error bars. Our code returns 1-σ error bars. To our best knowledge, this is the first time that formal errors of SED fits are obtained in a rigorous way. As an example of the soundness of the method, note that the obtained values of δ are affected by the largest errors when the distribution of the VHE data points is most irregular (e.g. states 4, 7).

We notice that the variability of Mrk 421 markedly differs from that of (e.g.) the other nearby HBL source, Mrk 501. The extremely bursting state of 1997 showed a shift of $\nu_{\rm s}$ and $\nu_{\rm c}$ by two and one orders of magnitude, respectively, suggesting a Klein-Nishina regime for the Compton peak (Pian et al. 1998). Based on the data analyzed in this paper, Mrk 421 displays (within our observational memory) a completely different variability pattern. However, one important similarity may hold between the two sources: based on eyeball-fit analysis of Mrk 501's SED in different emission states using a SSC model similar to the one used here, Acciari et al. (2010) suggest that $\gamma_{\rm br}$ does vary with L. If this correlation is generally true in blazars, the implication is that particle acceleration, providing fresh high-energy electrons within the blob, must be one defining characteristic of excited source states.

START
assign P_0, initial point in SSC parameter space, and $\Delta\chi^2_{\mathrm{NI}}$; set $c_{\mathrm{NI}} = 0$

$c_{\mathrm{NI}} = 0$

increase weight of steepest descent

compute $\chi^2(P_0)$
$\chi^2_0 = \chi^2(P_0)$

determine P, next point in SSC parameter space

compute $\chi^2(P)$

$\chi^2(P) \geq \chi^2_0$

$\chi^2(P) < \chi^2_0$

$\chi^2_0 = \chi^2(P)$
increase weight of inverse Hessian

NO

$\chi^2(P) - \chi^2_0 \leq \Delta\chi^2_{\mathrm{NI}}$

YES

output values of χ^2, SSC parameters and associated uncertainties
END

NO

YES

$c_{\mathrm{NI}} < 4$

$c_{\mathrm{NI}} = c_{\mathrm{NI}} + 1$
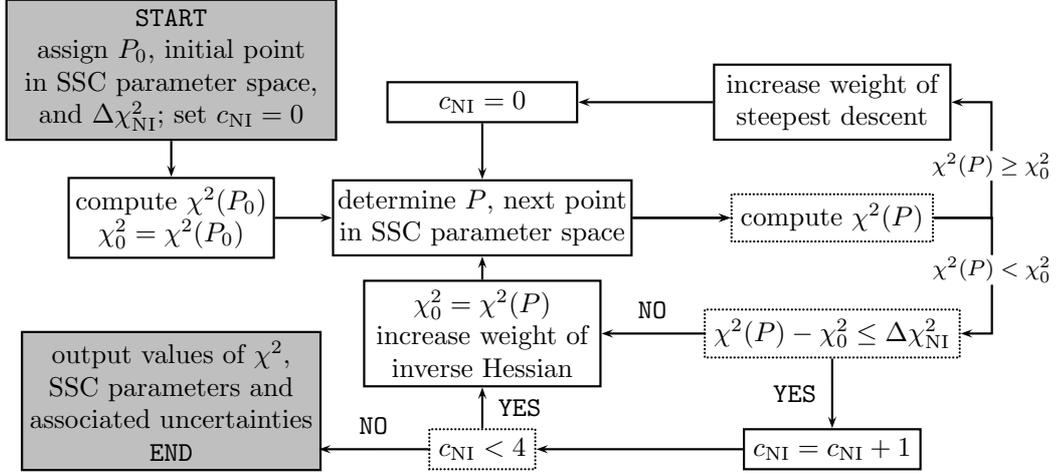
Fig. 1.— Flow chart of the minimization code.

Source	B	R	δ	χ^2_ν
	[gauss]	[cm]		
State 1	$(9 \pm 3) \times 10^{-1}$	$(9 \pm 4) \times 10^{14}$	$(2 \pm 0.5) \times 10^1$	0.84
State 2	$(8 \pm 6) \times 10^{-1}$	$(8 \pm 4) \times 10^{14}$	$(2.7 \pm 1.1) \times 10^1$	1.86
State 3	$(6 \pm 6) \times 10^{-2}$	$(2.0 \pm 1.5) \times 10^{15}$	$(1.0 \pm 0.5) \times 10^2$	0.91
State 4	$(1.21 \pm 0.16) \times 10^{-1}$	$(1.1 \pm 1.3) \times 10^{15}$	$(8 \pm 6) \times 10^1$	0.89
State 5	$(1.9 \pm 1.3) \times 10^{-1}$	$(10 \pm 4) \times 10^{14}$	$(7 \pm 5) \times 10^1$	0.67
State 6	1.0 ± 0.7	$(6 \pm 3) \times 10^{14}$	$(2.8 \pm 1.1) \times 10^1$	1.39
State 7	$(4 \pm 3) \times 10^{-2}$	$(2 \pm 5) \times 10^{15}$	$(8 \pm 7) \times 10^1$	1.61
State 8	$(6 \pm 3) \times 10^{-2}$	$(2 \pm 1.8) \times 10^{15}$	$(1.1 \pm 0.4) \times 10^2$	0.60
State 9	$(4 \pm 3) \times 10^{-2}$	$(2 \pm 4) \times 10^{15}$	$(1.2 \pm 1.0) \times 10^2$	0.85

Table 1: Best-fit single-zone SSC model parameters for the nine datasets of Mrk 421. States are named as in Fig. 2.
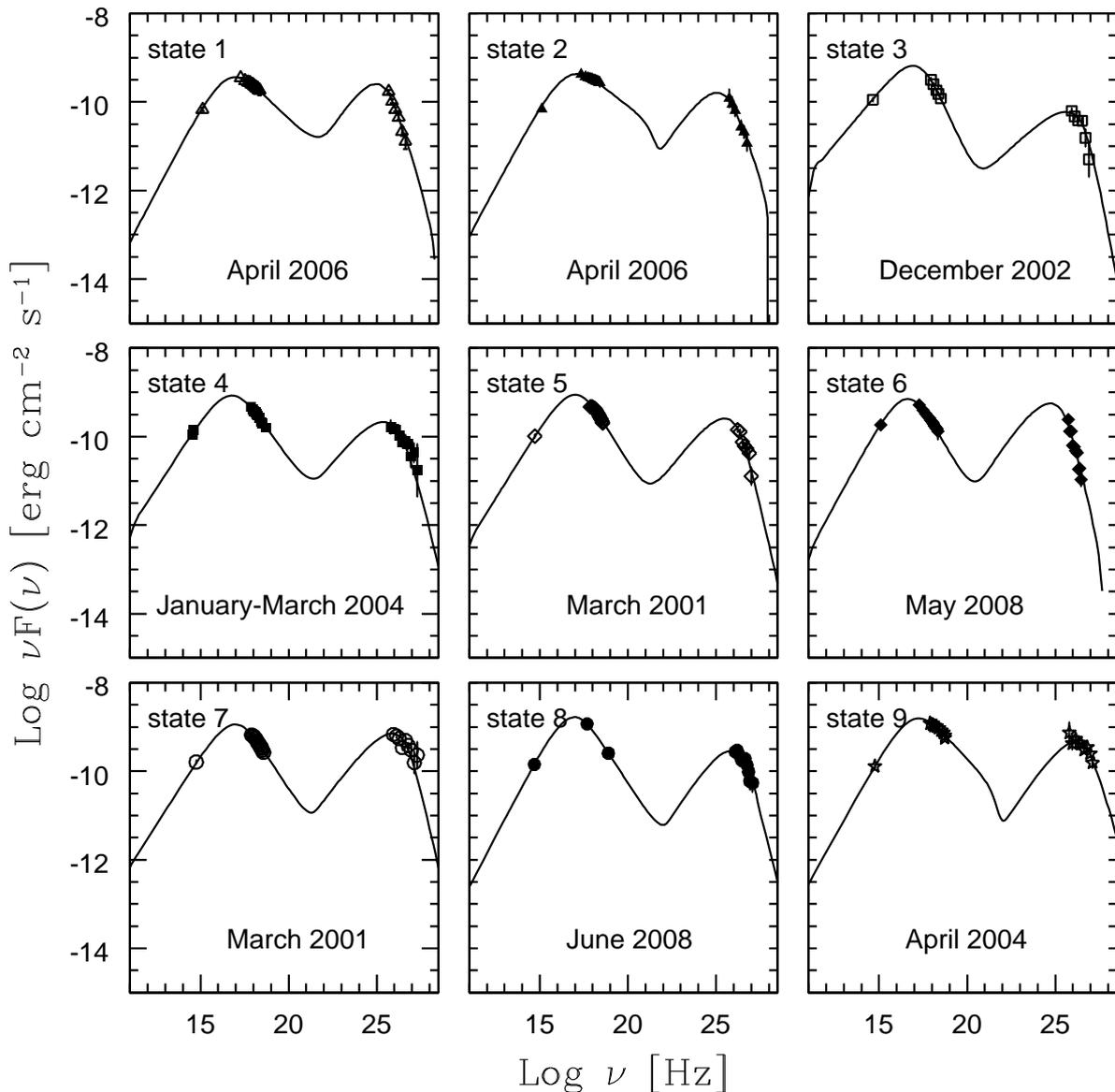
Fig. 2.— Best-fit one-zone SSC models for nine data sets referring to different emission levels of the HBL source Mrk 421. Source states are ordered by increasing model luminosity and data have been obtained as follows: state 1 (Acciari et al. 2009), state 2 (Acciari et al. 2009), state 3 (Rebillot et al. 2006), state 4 (Blazejowski et al. 2005), state 5 (Fossati et al. 2008), state 6 (Acciari et al. 2009), state 7 (Fossati et al. 2008), state 8 (Donnarumma et al. 2009), state 9 (Blazejowski et al. 2005).
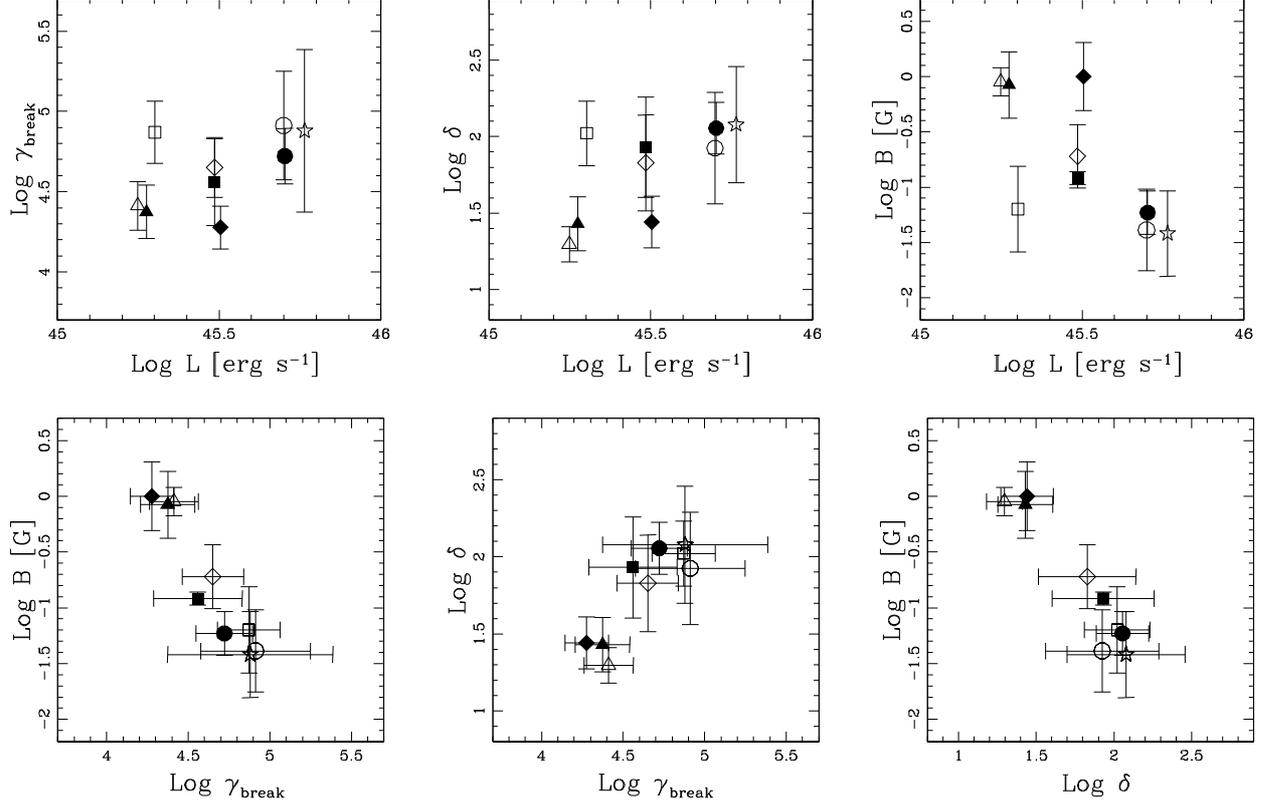
Fig. 3.— *Top.* Variations of the SSC parameters magnetic field B, Lorentz factor δ, and $\gamma_{\rm br}$ as a function of the model's bolometric luminosity. The other SSC parameters that are left to vary (R, n_e, γ_2, n_1, n_2 only show a scatter plot with the luminosity. *Bottom.* Correlations between B, δ, and $\gamma_{\rm br}$.

APPENDIX

A TOY MODEL MIMICKING THE PIECEWISE KS TEST RESULTS FOR THE SED'S

In this appendix we reproduce the outcome of the piecewise KS approach to goodness of fit using a simulated toy model. Let us consider the function $p(x; a, b, c) := ax^4 + bx^2 + c$. By using a pseudo-random generator, that produces uniformly distributed pseudo-random numbers in the interval $[0, 1]$ – which we will henceforth call $\mathtt{rnd}$ –, we generated $(x_i, y_i)_{i=1,\dots,5}$ pairs of points and $(w_i)_{i=1,\dots,5}$ numbers, where $x_i = -2.3 + 0.1 \cdot (i + 0.1 \cdot \mathtt{rnd})$, $y_i = p(-2.3 + 0.1 \cdot i; -1, 4, 0) + 0.2 \cdot \mathtt{rnd}$ and $w_i = \sigma_i^{-2}$ with $\sigma_i = 0.01 \cdot (\mathtt{rnd} + 1)$. These can be considered as 5 measurements around the $x = -2$ local maximum of the function $-x^4 + 4x^2$ with small uncertainties σ_i. We then generated another 5 pairs of points $(x_i, y_i)_{i=6,\dots,10}$ and $(w_i)_{i=6,\dots,10}$ numbers with $x_i = 1.7 + 0.1 \cdot (i + 0.1 \cdot \mathtt{rnd})$, $y_i = p(1.8 + 0.1 \cdot i; -2, 16, -14) + 0.3 \cdot \mathtt{rnd}$, $w_i = \sigma_i^{-2}$ and, finally, $\sigma_i = 0.1 \cdot (\mathtt{rnd} + 1)$, which again can be considered as 5 slightly randomized measurement around a maximum, but now the maximum of the function $-2x^4 + 8x^2 + 1$ and with much larger uncertainties that the first five ones.

By minimizing χ^2 we can fit the above set of 10 randomly generated data points versus the function $p(x; a, b, c)$. After obtaining the desired fitted parameters we calculate the residuals and, using the KS test, check if they are normally distributed. The KS test rejects normal distribution of the entire set of residuals at the 5% significance level. On the other hand, if we separately apply the KS test to the first, i.e. $\{i = 1, \dots, 5\}$, and the second, $\{i = 6, \dots, 10\}$, subset of residuals, the test confirms that the residuals are normally distributed. This exactly replicates the behavior we obtained in the SED fits.

Source	n_{e} $[\mathrm{cm}^{-3}]$	γ_{br}	γ_{max}	$\mathrm{n_1}$	$\mathrm{n_2}$
State 1	$(1.3 \pm 1.5) \times 10^3$	$(2.6 \pm 0.9) \times 10^4$	$(1.05 \pm 0.18) \times 10^7$	1.49 ± 0.19	3.77 ± 0.11
State 2	$(1 \pm 3) \times 10^3$	$(2.4 \pm 0.9) \times 10^4$	$(4.1 \pm 1.1) \times 10^6$	1.5 ± 0.3	3.62 ± 0.14
State 3	$(5 \pm 5) \times 10^3$	$(7 \pm 3) \times 10^4$	$(7 \pm 5) \times 10^7$	2.05 ± 0.10	4.8 ± 0.3
State 4	$(2 \pm 5) \times 10^3$	$(4 \pm 2) \times 10^4$	$(8.2 \pm 1.7) \times 10^6$	1.8 ± 0.3	4.11 ± 0.13
State 5	$(2 \pm 5) \times 10^3$	$(4.5 \pm 1.9) \times 10^4$	$(2.4 \pm 0.3) \times 10^7$	1.7 ± 0.3	4.3 ± 0.180
State 6	$(4 \pm 4) \times 10^3$	$(1.9 \pm 0.6) \times 10^4$	$(1.8 \pm 0.4) \times 10^6$	1.54 ± 0.11	4.37 ± 0.09
State 7	$(1 \pm 7) \times 10^3$	$(8 \pm 6) \times 10^4$	$(7 \pm 2) \times 10^6$	1.7 ± 0.4	4.23 ± 0.20
State 8	$(4 \pm 9) \times 10^1$	$(5 \pm 2) \times 10^4$	$(1.6 \pm 0.4) \times 10^7$	1.5 ± 0.2	4.22 ± 0.14
State 9	$(1 \pm 7) \times 10^2$	$(8 \pm 9) \times 10^4$	$(1.1 \pm 0.4) \times 10^7$	1.6 ± 0.5	3.9 ± 0.2

Table 2: Best-fit single-zone SSC model parameters for the nine datasets of Mrk 421. Numbering convention as in Fig. 2.

REFERENCES

Abdo, A.A., et al. (*Fermi*/LAT Collaboration) 2009, ApJ, 707, 1310

Acciari, V. A., et al. (VERITAS Collaboration) 2009, ApJ, 703, 169

Acciari, V.A. et al. (VERITAS and MAGIC Collaborations) 2010, ApJ, submitted

Aharonian, F., et al. 2007, ApJL, 664, L71

Albert, J., et al. (MAGIC Collaboration) 2007, ApJ, 669, 862

Anderhub, H., et al. (MAGIC collaboration) 2009, ApJ, 705, 1624

Andrae, R., Schulze-Hartung, T., & Melchior, P., 2010, arXiv:1012.3754v1 [astro-ph.IM]

Bednarek, W., & Protheroe, R.J. 1997, MNRAS, 292, 646

Blazejowski M. et al. 2005, ApJ, 630, 130

Celotti, A., & Ghisellini, G. 2008, MNRAS, 385, 283

Donnarumma I. et al. 2009, ApJ, 691, L13

Fossati, G., Buckley, J.H., Bond, I.H., et al. 2008, ApJ, 677, 906

Franceschini, A., Rodighiero, G., & Vaccari, M. 2008, A&A, 487, 837

Georganopoulos, M., & Kazanas, D. 2003, ApJL, 594, L27

Ghisellini, G., Celotti, A., & Costamante, L. 2002, A&A, 386, 833

Ghisellini, G., Tavecchio, F., & Chiaberge, M. 2005, A&A, 432, 401

Ghisellini, G., & Tavecchio, F. 2008, MNRAS, 386, L28

Giroletti, M., Giovannini, G., Taylor, G.B., & Falomo, R. 2006, ApJ, 646, 801

Henri, G., Pelletier, G., Petrucci, P.O., & Renaud, N. 1999, Astrop. Phys., 11, 347

Komissarov, S.S., Barkov, M.V., Vlahakis, N., & Kön
igl, A. 2007, MNRAS, 380, 51

Konopelko, A., Mastichiadis, A., Kirk, J., de Jager, O.C., & Stecker, F.W. 2003, ApJ, 597, 851

Krawczynski, H., Hughes, S.B., Horan, D., et al. 2004, ApJ, 601, 151

Mankuzhiyil, N., Persic, M., & Tavecchio, F. 2010, ApJL, 715, L16

Maraschi, L., et al. 1999, ApJL, 526, L81

Maraschi, L., Ghisellini, G., & Celotti, A. 1992, ApJ, 397, L5

Pian, E., et al. 1998, ApJ, 492, L17

Piner, B.G., Pant, N., & Edwards, P.G. 2010, ApJ, 723, 1150

Press, W.H., et al. 1992, Numerical Recipes (Cambridge: Cambridge University Press)

Rebillot, P. et al. 2006, ApJ, 641, 740

Tagliaferri, G., et al. (MAGIC collab.) 2008, ApJ, 679, 1029

Tavecchio, F., et al. 2001, ApJ, 554, 725

Tavecchio, F., Maraschi, L., & Ghisellini, G. 1998, ApJ, 509, 608 (T98)

Tavecchio, F., et al. 2010, MNRAS, 401, 1570

Vlahakis, N., & Königl, A. 2004, ApJ, 605, 656